Blast Response and Failure Analysis of a Segmented Buried Tunnel

Sivalingam Koneshwaran, David P. Thambiratnam*, Chaminda Gallage

Abstract

Underground tunnels are vulnerable to terrorist attacks which can cause collapse of the tunnel structures or at least extensive damage, requiring lengthy repairs. This paper treats the blast impact on a reinforced concrete segmental tunnel buried in soil under a number of parametric conditions; soil properties, soil cover, distance of explosive from the tunnel centreline and explosive weight and analyses the possible failure patterns. A fully coupled Fluid Structure Interaction (FSI) technique incorporating the Arbitrary Lagrangian-Eulerian (ALE) method is used in this study. Results indicate that the tunnel in saturated soil is more vulnerable to severe damage than that buried in either partially saturated soil or dry soil. The tunnel is also more vulnerable to surface explosions which occur directly above the centre of the tunnel than those that occur at any equivalent distances in the ground away from the tunnel centre. The research findings provide useful information on modeling, analysis, overall tunnel response and failure patterns of segmented tunnels subjected to blast loads. This information will guide future development and application of research in this field..

Keywords: explosion; finite element method; Fluid structure interaction; Arbitrary Lagrangian-Eulerian; tunnel; segment; reinforced concrete; saturated soil; damage; crack.

1. Introduction

An underground transit tunnel system provides a quick and cost effective alternative to surface rail or road transport. This system plays an important role in addressing the transportation needs in many cities. Terrorist attacks, such as the Belarus bombing in 2011, the Moscow metro bombing in 2004 and the London subway bombing in 2005, highlight that underground transit tunnels are vulnerable to potential terrorist attacks. Terrorist attacks on transportation tunnels must be closely considered for two reasons; i) the importance and centrality of such infrastructure, and ii) the level of public use. The failure of such underground tunnels would not only cause delays and transport network interruptions, but also result in severe loss of lives with considerable financial implications.

* corresponding author: tel: 61 7 31381467; fax: 61 7 3138 1170; e-mail: d.thambiratnam@qut.edu.au

A Vehicle Borne Improvised Explosive Device (VBIED) is commonly used as a weapon of terrorism to damage constructed facilities. VBIED can be carried in a wide range of vehicles such as cars, vans and trailers to transport a large amount of explosive without attracting suspicion. As the VBIED is relatively close to the ground surface, the explosion from the VBIED generates air-blast pressure as well as ground shock. Ground shocks travel through both soil and rock. In soil, the tunnel structure resists most of the ground shock, whereas in rock, the medium itself carries a large amount of the ground shock. As the shock wave intercepts the geostatic soil structure interface between the tunnel structure and surrounding soil, the tunnel experiences an effect of inertia lasting for a few milliseconds. The surrounding medium significantly constrains the tunnel motion. However, the tunnel response to the shock wave is similar to instantaneous vibration as damping from the surrounding medium is ineffective. The shock wave reaches the tunnel in a very short time before the damping activates itself (1). The tunnel can therefore exhibit excessive levels of stress affecting its structural integrity. This leads to a localized failure and potential collapse of the tunnel with serious consequences.

Bored tunnels with segmented tunnel lining are popular in underground railway systems. The tunnel lining is installed directly behind the Tunnel Boring Machine (TBM). The space between the bored soil/rock face and the lining is filled with annular concrete grout. The lining consists of prefabricated reinforced concrete segments placed together to complete one lining ring to span the circumference of the tunnel. The segments are connected to adjacent segments at contact joints by bolts which create an interlocking system providing the tunnel with resistance against external pressure from the surrounding ground. The stiffness of the joints determines the load transmission throughout the ring. The joints in both radial and circumferential directions consist of grooves to accommodate the elastomeric gasket that provides water-resistance. The bolts help to stabilise the ring during the grouting as well as to ensure the water-resistance by compressing the gasket in the years of service after construction.

The four key factors which affect the tunnel response under blast loading are: (i) surrounding ground type (ii) explosive mass, (iii) standoff distance and (iv) lining stiffness. Though the lining stiffness is the engineer’s choice, it may be difficult to evaluate how the tunnel response is influenced by its stiffness. The response of the segmented tunnel lining to the

blast loading is more complex than to other loadings such as geo-static and earthquake loadings. Performance of the segmented tunnels under static and earthquake loads has been the subject of several studies. However, there is inadequate information on response of bored tunnels to blast loading. It is therefore of interest to investigate the vulnerability of segmented tunnels to credible blast loading.

In this research field, there are no records on full-scale prototype field experiments investigating the tunnel response to surface blasts. Full-scale experiments are extremely risky and unattainable in civilian research as they involve the use of a large quantity of explosives. On the other hand, a limited number of studies have been conducted using scaled-down centrifuge modeling techniques to investigate the blast response of tunnels. Centrifuge modeling is beneficial for scale modeling of large-scale nonlinear problems in geotechnical engineering. Some previous studies (2-7) have successfully implemented the centrifuge modeling to simulate the blast response of buried structures. De (2, 3) conducted a series of centrifuge tests to study the surface blast effect on a buried cylindrical structure. Due to varying gravitational field in the test bucket, the centrifuge models are limited to smaller models which may not be adequate to predict the blast response of bolted joints in the segmental lining. Hayes (8) conducted the Conventional Weapon Effects Backfill (CONWEB) test series to investigate the blast response of buried reinforced concrete structures in differing backfills. This study used a small model of a reinforced concrete slab bolted to a reaction structure to study its blast response.

With the development of advanced computer simulations, several studies (3, 9-13) have simulated the blast response of transit tunnels using various numerical techniques. De (3) used the coupled fluid-structure interaction (FSI) approach in Arbitrary Lagrangian Eulerian (ALE) technique to study the surface blast response of a cylindrical structure using Autodyn. Yang et al. (10) examined the blast response of Shanghai metro tunnel using an advanced general purpose multi-physics computer software LS-DYNA (14). In this simulation, Eulerian soil elements were merged with Lagrangian tunnel elements at the common nodes. This simulation failed to consider the ground-lining interaction as the merged nodes were unable to simulate the separation, re-contact and sliding at the contact interface. Gui and Chien (13) investigated the performance of a bored tunnel passing beneath Taipei Shongsan airport subjected to a buried explosion using FLAC^{2D}, in which the problem was

conservatively simulated using a two dimensional blast wave propagation. Global response of the segmental lining to blast load is governed by the lining stiffness which depends on the elastic modulus of the material as well as on the geometric properties of the lining, such as cross-sectional area, joints and number of segments used to form a ring. The studies performed until to date have ignored the important aspect of the segment joints. Nasri Munfah (15) indicated that tunnels with precast segmental lining are more vulnerable to blasts than thick cast-in-place tunnels and hence the importance of considering the joints in such structures.

This paper treats the blast response of segmented bored tunnels subjected to a surface blast using ALE formulation incorporating fully coupled Fluid Structure Interaction (FSI) numerical techniques. In addition to previous validation of the modeling techniques carried out by the authors (16, 17), further validation is carried out in this paper using the results of the CONWEB test (8). These validations provide confidence in using these modelling techniques to investigate the blast response of reinforced concrete segments and bolted joints in the segmented tunnels. The influence of soil types as well as scale distances by varying the tunnel-explosive distances are studied with respect to different explosive weights. Three types of soils are considered first by varying the soil properties, followed by a study to predict the blast response of the segmented tunnel to different scale distances by varying the tunnel depth as well as the ground distance of explosive from the tunnel centreline. The study showed that the tunnel buried in the saturated soil was found to have the highest distortion and it suffered a large number of bolt failures. When the tunnel is subjected to a surface explosion, the tunnel depth as well as the ground distance of the explosive have significant influence on the tunnel response.

2. Material Constitutive Models

In this paper, a test described in the CONWEB test series (8) is simulated using the coupled FSI approach in ALE formulation. There are five material constitutive models applied for this simulation. Previous publications (17, 18) described the material models for air, explosive and reinforced steel. The material models for soil and concrete are explained in more detail below:

2.1. Soil

By evaluating several material models in LS-DYNA, MAT_FHWA_SOIL model is identified as a suitable soil model that includes strain softening, kinematic hardening, strain rate effects, element deletion, excess pore water effects and stability with no soil confinement (19, 20). There are a total of 25 material parameters in the FHWA soil model. Among those parameters, the model needs main parameters such as, mass density, specific gravity, bulk modulus, shear modulus, friction angle, cohesion and moisture content. These soil parameters are generally determined from various laboratory tests. Parameters required for describing strain softening, kinematic hardening, strain rate effects and pore water effects can be evaluated from laboratory tests and/or equations in the manual (19). Researchers Koneshwaran et al. (16-18), Jayasinghe et al. (21), Lee (22) and Ortman and Catherine (23) have employed this model for investigating the blast effect in saturated soil by utilizing the pore-water effect. Values recommended by Lee (22) are used in this study to include the strain softening, kinematic hardening and strain rate effects in the soil.

In the CONWEB test series, Hayes (8) considered a low shear strength and low seismic velocity reconstituted clay in backfill Test 1. The soil properties such as density, specific gravity and water content are shown in Table 1. The shear and bulk moduli were evaluated based on the density, seismic velocity and Poisson's ratio (24). The calculated bulk modulus is consistent with the volumetric strain changes observed between pressure steps (25). The cohesion and friction angle were based on the modified material properties described by Baylor (25).

Table 1: Material properties of reconstituted clay

Parameters	Value
Density, ρ	1.96 g/cm^3
Specific gravity, Gs	2.71
Shear modulus, G	36.7 MPa
Bulk modulus, K	171.4 MPa
Cohesion, C	2.275e-2 MPa
Friction angle, ϕ	22.3^o
Moisture content, w	23.3%
PWD_1	6.30e-03 MPa^{-1}
PWD_2	5.61e-02 MPa^{-1}

In order to include the pore-water effects, the parameters PWD_1, PWD_2 and K_{sk} must be active in the input material card (19). PWD_1 defines the stiffness of the soil by adjusting the bulk modulus before the air voids collapse. PWD_2 computes the pore-water pressure in the soil before the air voids collapse. As recommended by Lee (22), K_{sk} is the volumetric strain factor which varies between 5% and 20% of material bulk modulus. Degree of saturation of the reconstituted clay was evaluated as 89.6% based on the density, specific gravity and water content. PWD_2 was determined for partially saturated soils using the equation in reference (19). PWD_1 was estimated based on best fit material analysis graph using the free-field blast simulation.

2.2. Concrete

Dynamic performance of concrete structures subjected to blast effects is a complex nonlinear and rate-dependent process, in which the apparent concrete strength can increase significantly. LS-DYNA material library has several advanced constitutive material models developed to simulate the concrete material behavior. However, in many circumstances, the necessary material parameters for the concrete cannot be found in the literature. This study utilized a common material model *MAT_WINFRITH_CONCRETE (14) which has the automatic generation capability of concrete law parameters.

This is a simple input concrete model which requires the unconfined compressive strength and tensile strength. This model is based on the shear failure surface proposed by Ottosen (26) and includes the strain rate effects and strain softening in tension by incorporating crack opening width or fracture energy. For known concrete weight and unconfined concrete compressive strength, Young's modulus (*E*) is calculated from an equation recommended by ACI Committee 318 as below:

$$E = 33w^{1.5}\sqrt{f_c'} \qquad \text{Eq. 1}$$

where: *w* is the concrete weight in lb/ft^3 and f_c' is the compressive strength of normal strength concrete in *psi.*

The fracture energy for the concrete containing limestone aggregate, used in the experiment, was considered as 70N/m (27). Table 2 shows the material parameters adopted in the simulation of backfill tests.

Table 2: Material properties of concrete

Parameter	Value
Density (g/cm3)	2.24
Young's modulus (GPa)	29.3
Unconfined compressive strength (MPa)	42.0
Poisson's ratio	0.19
Uniaxial tensile strength (Mpa)	3.54
Fracture energy per unit area (N/m)	70.0
Maximum aggregate size (mm)	9.5

3. Numerical Simulation of the CONWEB test

The numerical model consisted of four main components which are the buried explosive, soil, air and the test structure. As described in Koneshwaran et al. (18), a quarter of each of the soil and explosive and a half the structure were modelled as shown in Fig. 1.

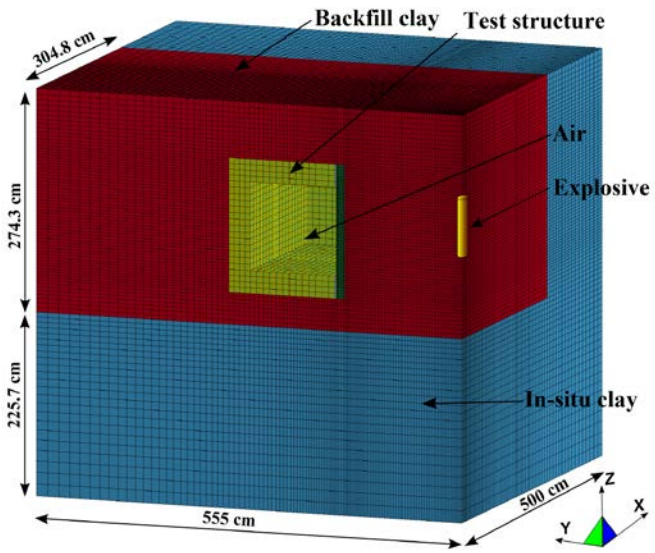

Fig.1: A half symmetry numerical model

The reaction structure and the test slab were modelled using the eight-node hexagonal solid elements with Lagrangian meshes. The soil and air within the interior volume of the structure were modelled using the eight-node hexagonal solid elements with Eulerian meshes. The cylindrical explosive was defined into the soil mesh using INITIAL_VOLUME_FRACTION _GEOMETRY by specifying its radius, height and detonation point. A series of mesh sensitivity studies provided an appropriate mesh refinement to capture the detonation process and subsequent response of the structure. The soil was refined with a gradual increase in mesh size in both X and Y directions from the explosive center. The size of the smallest

element in the central part of the explosive was 2.25cm x 2.25cm x 3.0cm. The interface between the backfill soil and the in-situ clay were modelled with merged nodes. Since material properties were not available for the in-situ clay, it was assumed to be the same as the backfill material.

In the simulation, a fully coupled FSI approach combining both Lagrangian and Eulerian solvers was adopted to allow for the incorporation of the essential processes using CONSTRAINED_LAGRANGE_IN_SOLID. Nodes in the symmetry boundaries of XZ and YZ planes were constrained in their normal directions. The bottom of the mesh was modelled as fixed in all directions. Along the infinite boundary of the entire computational domain, non-reflecting boundaries were set as flow out boundaries to avoid shock wave reflection.

Fig.2 illustrates half of the test structure which was modeled with appropriate boundary conditions at the symmetry planes. The reinforcement details described in the CONWEB test (8) was simulated in the model. The reinforcement steel and bolts were modeled using Hughes-Liu beam elements with cross sectional integration. This is a simple and computationally efficient beam element that is compatible with most material types. All reinforcing beam elements were merged to the solid concrete elements at the common nodes. The test slab was modeled with a very fine mesh to achieve adequate accuracy of the deflection. Minimum of two hexahedral elements were specified for the reinforcement cover. There were 72960 solid elements in the test slab attached to the steel plate with 20 bolts. The simulation was free from pretension in bolts. In the test slab, bolts were modeled as discrete elements immersed in the slab meshes using the *CONSTRAINED_LAGRANGE_IN_SOLID coupling. In the steel plate, the same nodes were shared for a perfect bond between the steel plate and bolts. The *CONTACT_AUTOMATIC_SINGLE_SURFACE contact was also used to define the interface between the test slab and the steel plate.

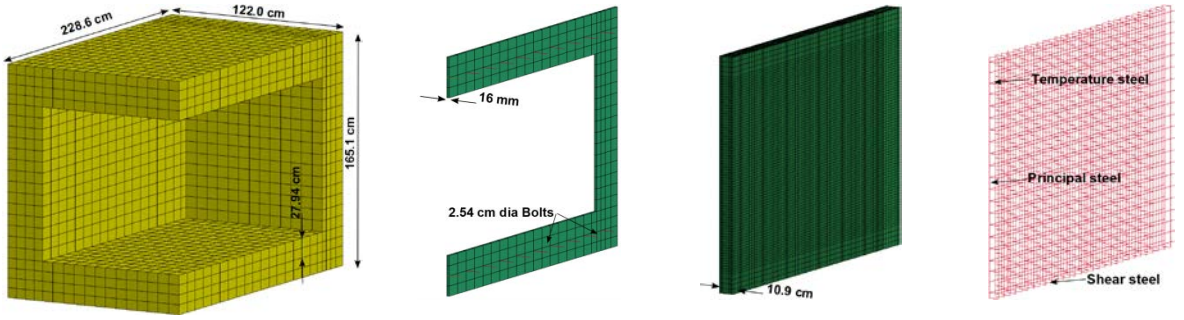

(a) Reaction structure (b) Steel plate/bolts (c) Test slab (d) Reinforcement

Fig.2: Test structure

As the steel plate was cast integrally together with the reaction structure, the perfectly bonded 'no slip' condition was simulated between the steel plate and reaction structure. The material properties for the steel plate were specified by Bessette (24) and the steel was modeled with *MAT_PLASTIC_KINEMATIC material model. The reaction structure was a heavily reinforced thick concrete structure (8). Since there were no reinforcement details available, for simplicity, the reaction structure was modeled as a smeared concrete as also adopted by others (10). Material properties for all other materials were outlined in the section 2.

3.1. Numerical validation of CONWEB test

The experiment was simulated using LS-DYNA with Shared Memory Parallel (SMP) processing. The simulation was conducted in two stages of stress initialization and blast analysis. The model was initialized using a time-dependent mass damping option *DAMPING_GLOBAL to impose near-critical damping until the preload was established. Upon initializing the model, the blast was initiated.

3.2. Test slab response

The response of the test slab under buried blast was investigated. Fig.3 shows the progress of the slab deformation as the shock wave travels through the structure over 20ms of duration. After igniting the explosive at 300ms, blast induced shock waves traveled through the soil and compressed the test slab surface. The shock wave front impacted the exterior surface of the slab at 303.1ms.

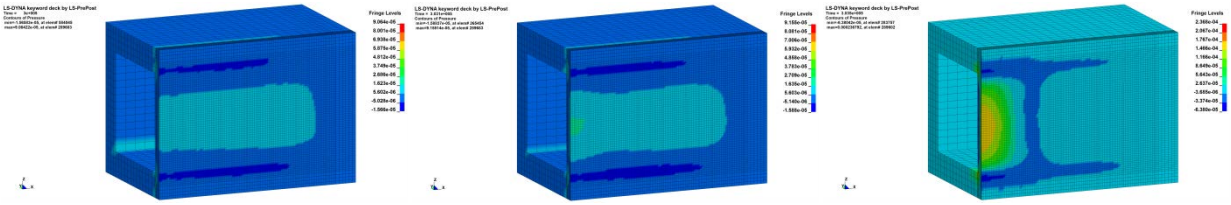

(a) t=300 ms (b) t=303.1 ms (c) t=303.5 ms

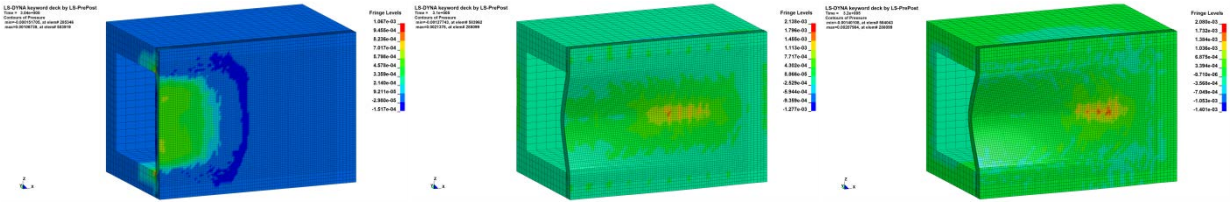

(d) t=304 ms (e) t=310 ms (f) t=320 ms

Fig.3: Progress of test slab deformation

The slab displayed some kind of breaching failure at its center and the failure extended away from the center, as the shock wave progressed through the slab. Before the reinforcement bars near the center of the slab failed, those at the top and bottom support edges broke due to both tensile failure and shear failure mechanisms. Fig. 4 displays the broken reinforcement at the end of the simulation. The observed damage in the reinforcement is similar to that in the experiment as described by Hayes (8). Along the exterior edges of the support, there was a series of separation between the slab and steel plate due to both localized rotation and deformation of bolts.

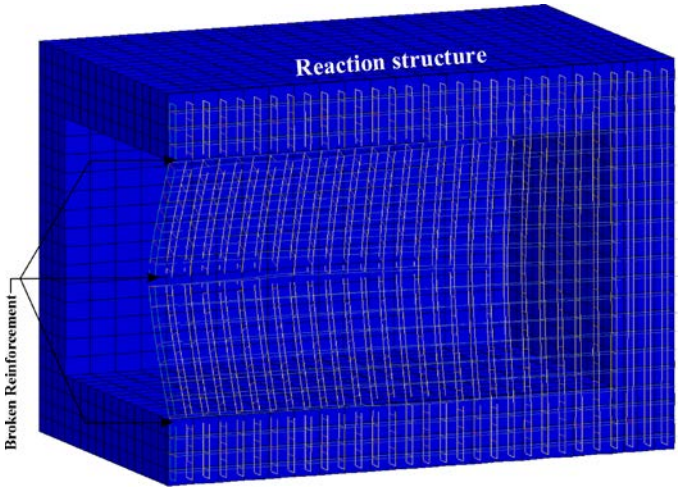

Fig.4: Broken slab reinforcement

Crack opening capability in the concrete material model illustrate the failure or damage in the slab. Cracks first appeared in both interior and exterior surfaces after 4ms of the explosion as

shown in Fig.5(a) and 5(d). Fig 5 shows that most of the damage of test slab occurred within a very short period of time from the excessive impact of blast pressure. During the early stages of the simulation, cracks were vertical and parallel to the principal steel. A number of diagonal cracks initiated on the interior slab surface. At later stages, large number of diagonal cracks emanated from the bolt points which act as a stress initiating points from the deformation mechanism. The interior and exterior views of the slab damages, crack patterns and deformed shapes at the end of the simulation are similar to those observed in the CONWEB test (8).

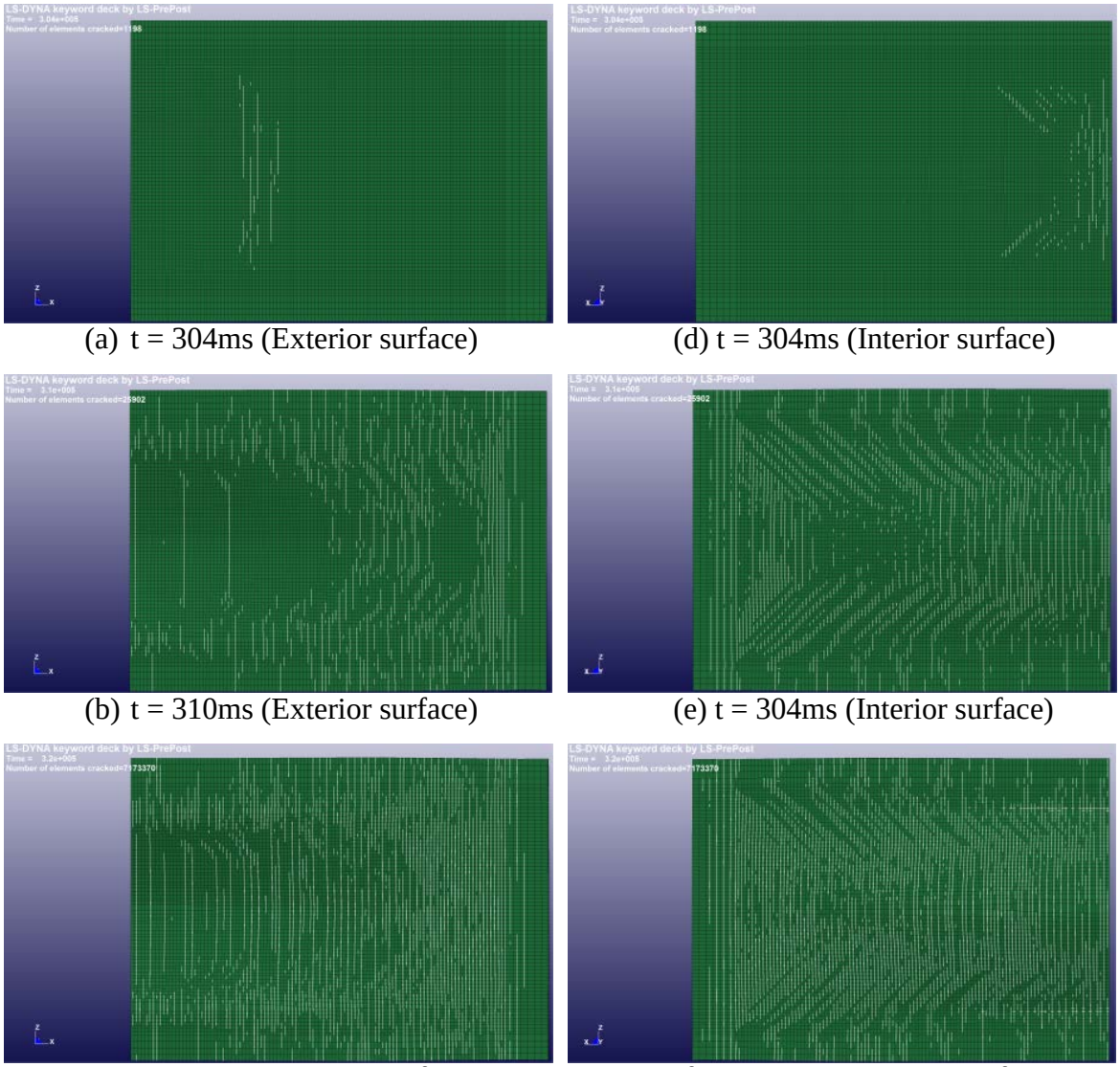

(a) t = 304ms (Exterior surface) (d) t = 304ms (Interior surface)

(b) t = 310ms (Exterior surface) (e) t = 304ms (Interior surface)

(c) t = 310ms (Exterior surface) (f) t = 320ms (Interior surface)

Fig.5: Propagation of cracks on test slab surfaces

In order to compare the displacement history of the slab with the results from the CONWEB test, six gauges mounted on the slab surface are considered as reported in CONWEB test (8).

Fig.6 compares the present results for displacement histories at the six gauges with those from the CONWEB test (8). It shows that the numerical simulations of the displacements compared well with the corresponding experimental displacements and are within the deviation limits with few exceptions. At first, a small lag in the time of shock wave arrival was observed in the simulation. This could be due to the small deviation in soil material properties evaluated based on several assumptions and empirical formulae. Secondly, comparisons clearly show that displacement-time responses are slightly steeper during the first half of the simulation. The displacement-time response is dependent on the Young's modulus of the concrete used in the CONWEB test (8) where the concrete was made with a limestone aggregate. Since there are no records of stress-strain relationship available for the concrete containing limestone aggregate, Young's modulus used in the present simulation was evaluated based on Eq. 1. As highlighted by Oluokun et al. (28), this equation predicts less accurate values of the Young's modulus.

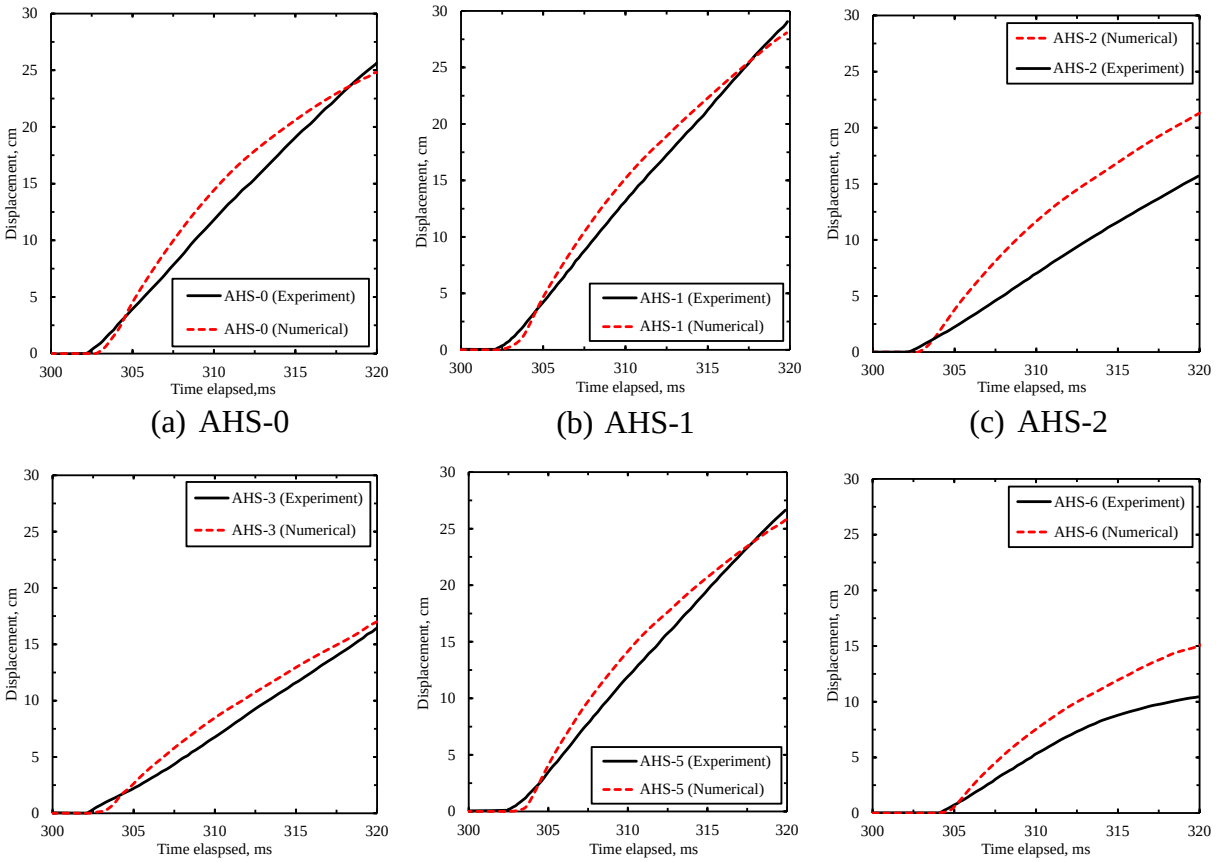

(a) AHS-0 (b) AHS-1 (c) AHS-2

(d) AHS-3 (e) AHS-5 (f) AHS-6

Fig.6: Comparison of displacements

Along the transverse direction at gauges AHS-1 and AHS-5 numerical predictions are reasonably close to the experimental values, but at AHS-6 they seem to diverge with time. The reason for this discrepancy is unclear and it was also observed in the numerical simulation reported by Bessette (24). Numerical predictions are also reasonably close to the experimental values along the vertical center line of the slab, except at AHS-2 where there is over-prediction of the results. This was also observed in Bessette (24). By comparing experimental displacements from surrounding gauges, this variation at AHS-2 could be due to possible disturbance of the gauge caused by excessive cracking near the center of the slab. Overall, the numerical displacements are reasonably close to the experimental values at many locations. The numerical results of reinforcement bar failure, crack patterns in the slab and slab deflections agree reasonably well with those from the experiment and provide adequate confidence in the present modelling techniques which are then applied to study the blast response of buried tunnels with bolted segments.

4. Blast Response of Segmented Tunnels in Different Soils

In bored tunnel construction, the soil types can vary along the length of the tunnel. This section investigates the blast response of a segmented tunnel buried in different soil types. Three types of soils considered by Jayasinghe et al. (29) to investigate the blast effect on buried piles are used in this study.

4.1. Peak pressures in various soil types

Table 3 presents the properties of the three soil types - saturated soil, partially saturated soil and dry soil. As also done by Jayasinghe et al. (29), a similar free-field study was first conducted. The free-field peak pressure attenuation responses for these three soils were consistent with the plots presented by Jayasinghe et al. (29). Fig.7 shows comparison of the peak pressure attenuations for the three types of soils as a function of scaled distances. It shows that both the soil type and the degree of water saturation play a large role in determining the peak pressures. The comparison shows that higher peak pressures occur in the saturated clay soil.

Table 3: Soil properties for numerical simulation (29)

Soil properties	Saturated soil	Partially saturated soil	Dry soil
Composition	Clay	Sand & Clay	Sand
Density	2065 kg/m^3	1960 kg/m^3	1450 kg/m^3
Degree of saturation	100%	85% (V_a> 4%)	0%
Seismic velocity	1575 m/s	500 m/s	175 m/s

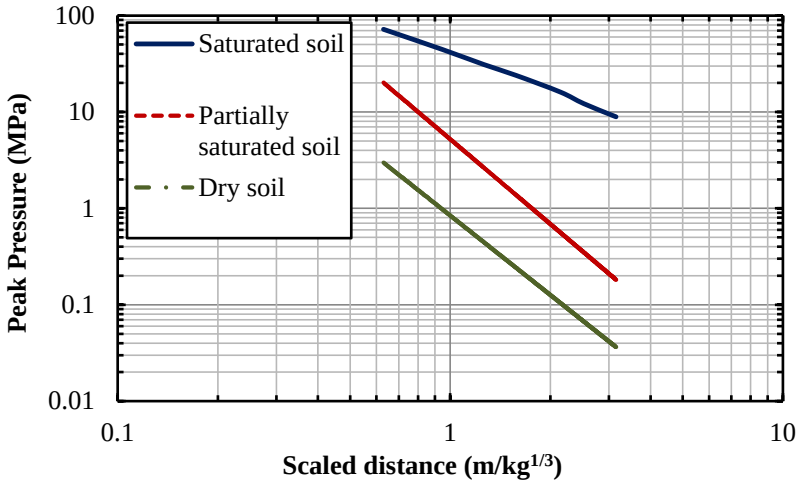

Fig.7: Comparison of free-field peak pressure

4.2. Description of segmented tunnel

As described in Fig. 8, a common single tube railway tunnel system (30) was considered with a 150mm thickness annulus concrete grout of concrete grade 15 around the tunnel. The inner diameter and the thickness of the tunnel lining were 5.8m and 275mm respectively. The segment was 1.4m length in longitudinal direction. As illustrated, the segments were rotated from ring to ring by 22.5 degree angle to the tunnel centreline (CL). Both radial and circumferential joints were flat and reinforcement details are described in Fig. 8.

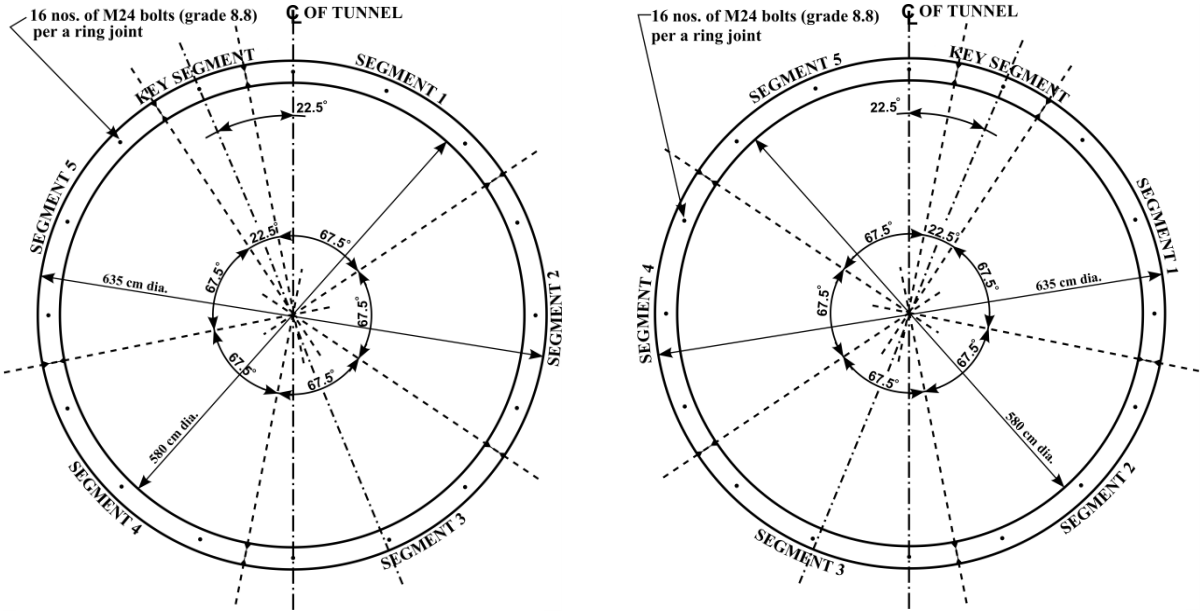

(a) Key segment: left-hand CL (b) Key segment: right-hand CL

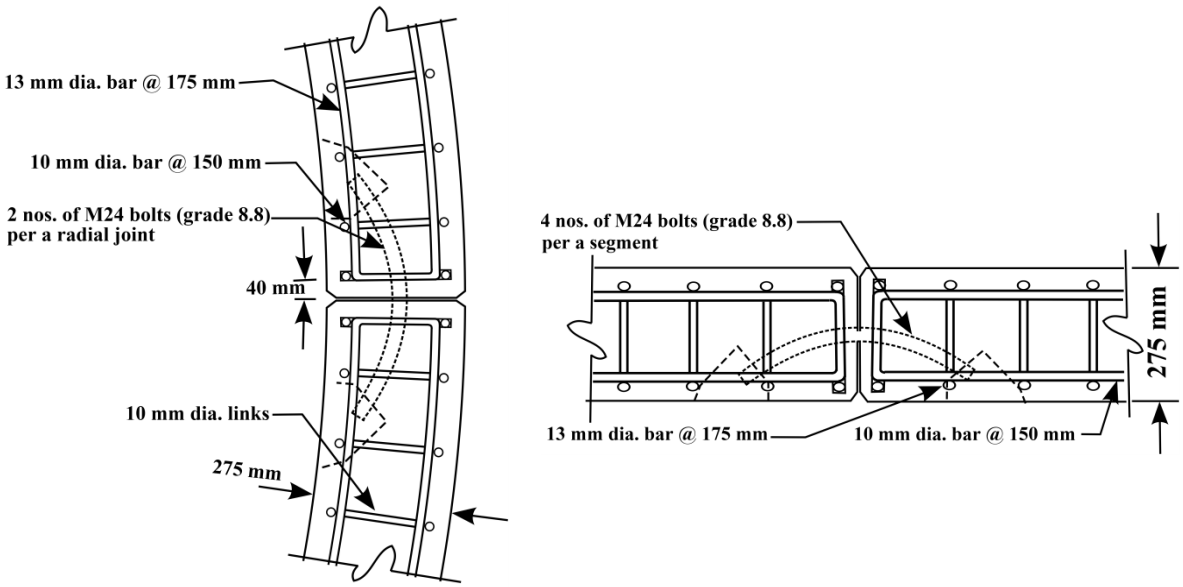

(c) Radial joint (d) Circumferential joint

Fig.8: General arrangement of segments

4.3. Modelling information

Fig. 9 represents the three dimensional numerical model to study the effects of surface blast loading on tunnel response under the influence of the soil properties. By considering the symmetries, half of the geometry was modelled with a cylindrical explosive on the ground surface. The annulus gap grout achieved a full round embedment with the surrounding soil. Therefore, the interface between the grout and soil was modelled using merged nodes.

However, the interface between the segments and grout was modelled using the penalty based contact surface-surface type. Apart from the geometrical aspects of segments, modeling of segments and its reinforcements were similar to modeling the test slab and reaction structure (18).

The soil properties were changed to investigate their effects on the different aspect of the tunnel response. A number of blast cases (1 to 5) were considered by varying the mass of the cylindrical disk type explosive from 250 to 1250 kg of TNT, by equal amounts of 250 kg, for a given tunnel depth of 6.35 m.

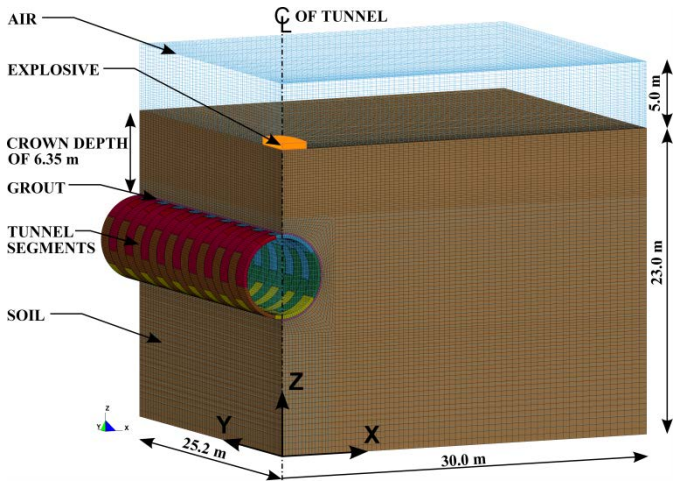

Fig. 9: A half symmetrical numerical model

4.4. Blast response of RC segmented tunnel

Prior to the blast, the model was brought to equilibrium under gravity loading. As the simulations are quite expensive in terms of computational time and memory space, the process of capturing the blast responses was recorded over 300ms of duration. Blast induced tunnel deformations were three dimensional. However, as the tunnel is naturally restrained along the direction of tunnel axis, in-plane (ZX plane) deformation of the ring immediately below the explosive is critically more important than out of plane deformation in the blast analysis. Before the blast, tunnel exhibited a gravity-induced elastic diametric distortion. After the blast, the diametric distortion of the tunnel is significant as it changed its shape to ovalisation before the tunnel failed due to either the joint distortion or excessive cracks in the segmented tunnel. Blast induced tunnel in-plane deformation can be expressed by Eq. 2.

$$D(t) = D_0 + \Delta(t) \qquad \text{Eq. 2}$$

where: $D(t)$ is the diameter of deformed tunnel at time t, D_0 is the initial diameter of the tunnel and $\Delta(t)$ is diametric distortion at time t.

Fig.10 shows the time histories of the diametric distortion which resulted from the displacement of the tunnel crown with respect to the tunnel invert in different soils. The figures illustrate that the tunnel experienced unrecoverable deformation in all the cases. In general, after first peak, the tunnels were subjected to a series of noticeable fluctuations in distortion before steadying to residual distortions. It can be seen that the amplitudes of the fluctuations depend on the soil type. For instance, the tunnel buried in the partially saturated soil displayed a quicker residual distortion than that in the other two soils. It also displayed smaller diametric distortion than in the dry soil. This could be due to inclusion of water in pore spaces of the soil skeleton reducing the response of the tunnel to blast loads as the partially filled pore water acts as a liquid damper.

The tunnel buried in the dry soil suffered higher peak diametric distortions than the tunnel in the partially saturated soil. As expected, the tunnel buried in saturated soil produced considerably large peak distortions (up to load case 3). Beyond load case 3 in the saturated soil, the key segment in the immediate plane disintegrated from the neighbouring segments due to the drifting response resulting from the bolt failure and this may lead to progressive collapse of the tunnel structure. This is expected as a sudden increase in the pore water pressure within the soil due to blast loading caused reductions in both effective normal and shear stresses in the soil surrounding the tunnel structure. As a result, the soil lost its ability to hold the tunnel and was able to offer only an insignificant amount of resistance to the blast loading. The tunnel structure therefore carried a large amount of the blast loading which led to severe structural failure in the tunnel than in the other two soil types.

Therefore, it is recommended that the tunnels should be buried above the ground water table. However, this may not be practicable because of minimum soil cover requirement and variation of the ground moisture level with seasonal changes.

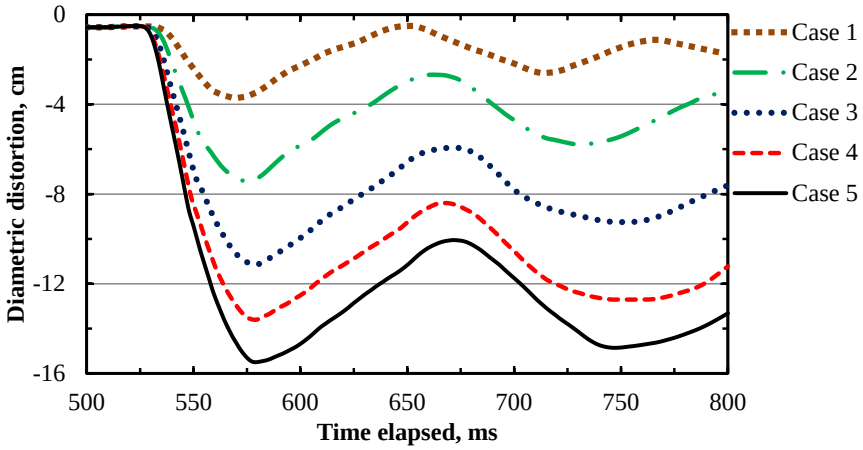

(a) Diametric distortions in dry

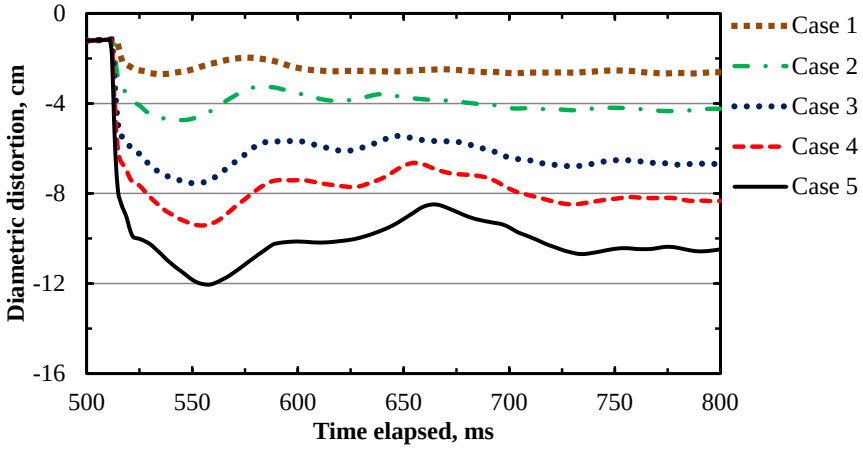

(b) Diametric distortions in partially saturated soil

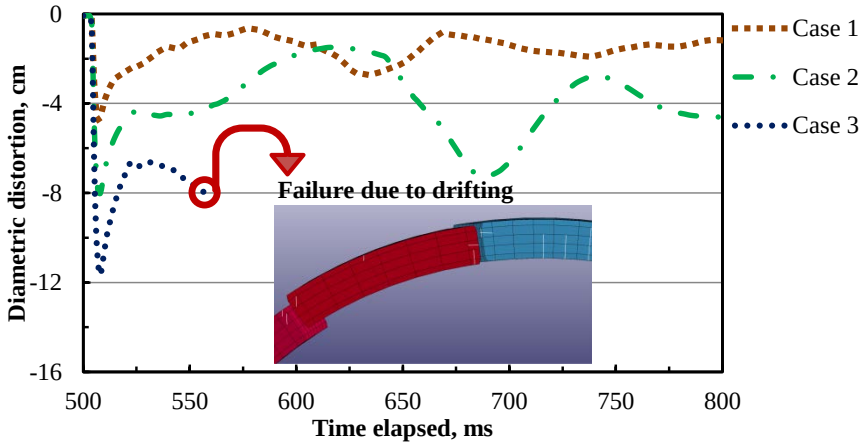

(c) Diametric distortions in saturated soil

Fig.10: Diametric distortion in different soil types

Table 4 compares the number of radial bolt failures during the first peak distortion and at the end of the simulation of the tunnel in different soils. There were no bolt failures in the tunnel buried in the dry soil for all load cases. Though the tunnel in the partially saturated soil

displayed bolt failure for the highest load cases 4 and 5, in-plane tunnel profile was not affected by any form of drifting responses. For the saturated soil, there were bolt failures in all load cases. A comparison of peak pressure attenuations study, as shown in Fig. 7, illustrates that the peak pressure of the saturated and partially saturated soils were 40 and 5 times the peak pressure of the dry soil at the depth of 6.35m for load case 1 (scaled distance ≈ 1.0m/kg$^{1/3}$). As a result, a large number of radial bolts failed in the saturated soil by the high intensity compressive blast wave impacting the tunnel crown. Immediately after the first peak distortion in load case 3, all radial bolts failed around the key segment which was drifted upwards due to the presence of blast induced negative pressure at the tunnel crown. The number of bolt failure at the end of the simulation shows a rapid increase from load case 2 to 3 for the saturated soil.

Table 4: Numbers of radial bolt failure

	Numbers of radial bolt failure during the first peak distortion / end of the simulation(@ 800ms)				
	Case 1	Case 2	Case 3	Case 4	Case 5
Dry	0 / 0	0 / 0	0 / 0	0 / 0	0 / 0
Par. saturated	0 / 0	0 / 0	0 / 0	3 / 3	3 / 3
Saturated	1 / 4	4 / 11	7 / 32	9 / 41	11 / 51

5. The Effect of Tunnel Depth and Stand-off Distance in Blast Impact

There are numerous empirical relationships relating stand-off distance to blast effects from various explosive weights for free-field explosions. However, the relationship between stand-off distance and the segmented tunnel response due to a surface blast are not reported. There is no established guidance for predicting either the tunnel response or the characteristics of the blast loading. In this section, the effects of tunnel depth, ground distance and explosive weight on the tunnel response in the saturated soil are studied. Fig. 11(a) shows that the tunnel depth is varied from 6.35m (= 1D) to 12.70m (= 2D), and the ground distance is varied from the tunnel centreline to 12.70m (= 2D) as shown in Fig. 11(b).

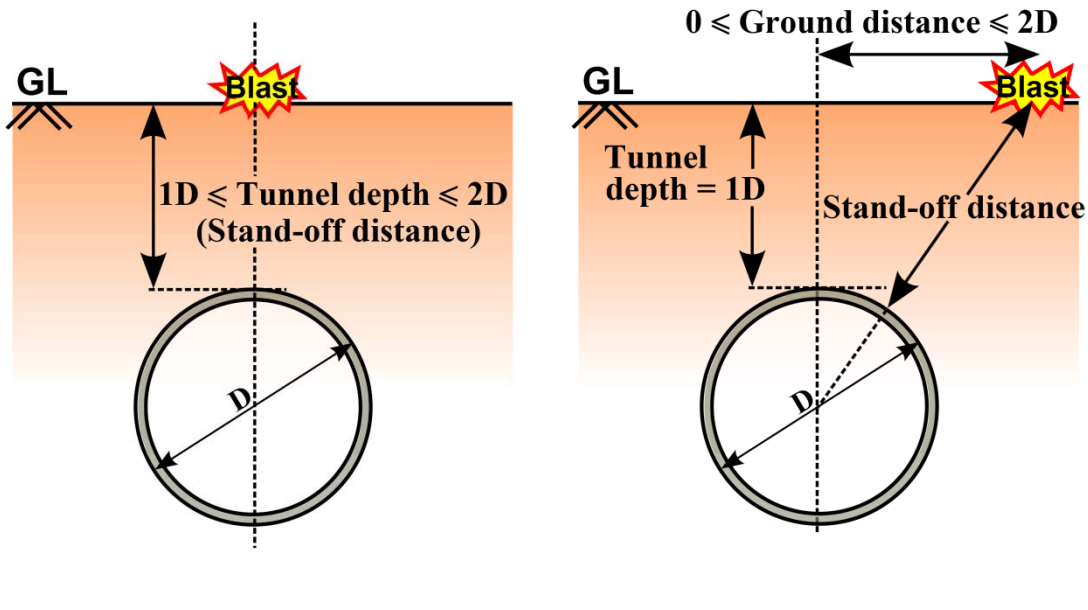

(a) Variation of tunnel depth of

(b) Variation of ground distance

Fig. 11: Variation of tunnel depth and ground distance

Cracks in segments, bolt failure and drifting response are considered in this study as critical factors to evaluate the blast performance of the tunnel structure. The damage state of tunnels can be divided into the following four groups:

1. no damage (the tunnel is considered to behave elastically with some minor cracks in segments (maximum crack width < 0.3mm (31)) and no bolt failure);
2. slight damage (a small number of cracks exceeded the crack limiting value of 0.3mm and a few bolts failed at joints, but the drifting response is insignificant);
3. moderate damage (a large number of cracks exceeded the crack limiting value of 0.3mm, a large number of failed bolts triggered significant drifting or sliding of segments at joints, however, the tunnel remains functional by keeping the in-plane tunnel profile due to hoop compression);
4. severe damage or collapse (formation of fully depth cracks, large number of bolt failures and resulting in large drifting between segments).

The damage state increases with an increase in the intensity of the shockwave impacting the tunnel. Low-energy blast impacts little or no damage in the tunnel lining while high-energy blast impacts cause moderate to severe damage.

In the present study, more than 30 models were considered to identify critical situations under the influence of tunnel depth, ground distance and explosive weight, but only a few important results are shown in this section. Fig. 12 illustrates the failure modes of the tunnel under a load of 750kg of TNT (Load case 3) at different tunnel depths. It can be seen that the tunnel depth showed significant influence on the failure modes of the tunnel when the surface explosive was directly above the tunnel crown. For the tunnel depth of 6.35m (1D), the tunnel was severely damaged with wide and deep cracks, segments were crushed and drifted away from the adjacent segments and a large number of bolts failed as shown in Fig. 12(a). There was not much difference in the tunnel buried at depth 2D in terms of number of bolt failures. However, when referring to damage due to the crack, a significant change in the crack response retained the in-plane tunnel profile without large drifting between segments as displayed in Fig. 12(b). The damage level corresponds to the state of "moderate damage". As the depth further increases to 2D, the tunnel responded with very small cracks, in which the maximum crack width was 0.24mm, less than the crack limiting value of 0.3mm. From this point of view, it is appropriate to say that the tunnel is safe with "no (serious) damage".

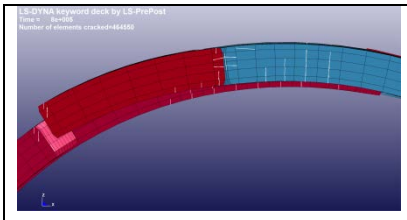	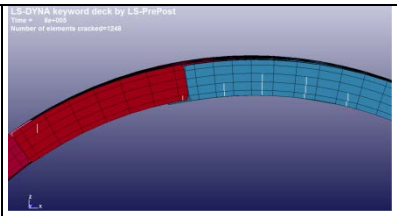	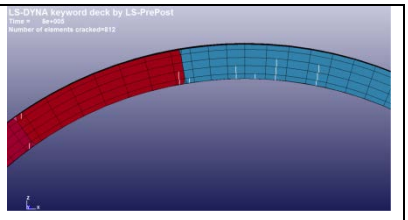
Max. crack width = 2.20mm	Max. crack width = 0.57mm	Max. crack width = 0.24mm
Nos. of cracks (>0.3mm) = 81674	Nos. of cracks (>0.3mm) = 60	Nos. of cracks (>0.3mm) = 0
Nos. of bolt failure = 35	Nos. of bolt failure = 10	Nos. of bolt failure = 0
(a) Severe damage	(b) Moderate damage	(c) No damage

Fig. 12: Failure modes of the tunnel for different tunnel depths (load case 3)

Table 5 compares the damage scenarios for the tunnel based on the drifting response, maximum crack width and corresponding numbers of bolt failures under a series of explosives from case 1 (250kg of TNT) to case 5 (1250kg of TNT). For the first two damage states, the drifting response is insignificant, although few radial bolts failed resulting in a "slight damage" state. The combined effect of the cracking and bolt failure influenced the drifting response in "severe damage" state where the crown segments were severely drifted

with respect to the adjacent segments in both longitudinal and transverse directions. This resulted in a significant number of circumferential bolt failures beyond load case 3 for the tunnel depth of 6.35m (1D). There were no circumferential bolt failure in both depth 1.5D and depth 2D for all load cases. The segments were slightly drifted and stabilized to a "moderate damage" state while maintaining the in-plane tunnel profile.

Table 5: Maximum crack width in mm / nos. of bolt failures

Depth	Case 1	Case 2	Case 3	Case 4	Case 5
Depth 1D	0.62 / 4	0.97 / 11	2.20 / 35	3.00 / 45	4.40 / 63
Depth 1.5D	0.20 / 0	0.37 / 2	0.57 / 10	0.60 / 17	0.90 / 32
Depth 2D	0.15 / 0	0.21 / 0	0.24 / 0	0.36 / 2	0.54 / 6

: No damage : Slight damage

: Moderate damage : Severe damage

Fig. 13 compares the failure modes of the tunnel under load case 3 at different ground distances for a specified tunnel depth of 6.35m (1D). The cracks on the segments were observed from different ground distances. The ground distance from the explosive has a significant influence on the damage response, which is similar to the tunnel response due to the variation of the tunnel depth. As compared in Table 6, there were no bolt failures at a distance of 12.70m (2D) for load cases 1 to 4. In load case 5 for a distance 2D, the tunnel displayed considerable drifting between segments.

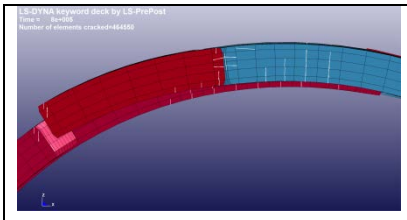	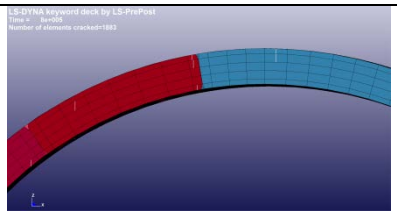	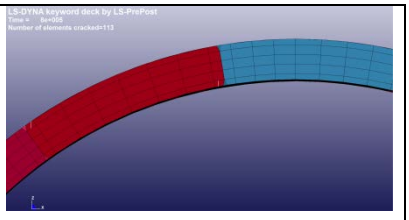
Max. crack width = 2.20mm	Max. crack width = 0.40mm	Max. crack width = 0.10mm
Nos. of cracks (>0.3mm) = 81674	Nos. of cracks (>0.3mm) = 34	Nos. of cracks (>0.3mm) = 0
Nos. of bolt failure = 35	Nos. of bolt failure = 4	Nos. of bolt failure = 0
(a) Severe damage	(b) Moderate damage	(c) No damage

Fig. 13: Failure modes of the tunnel under different ground distances (load case 3)

Table 6: Maximum crack width in mm / nos. of bolt failures

Distance	Case 1	Case 2	Case 3	Case 4	Case 5
Distance 0	0.62 / 4	0.97 / 11	2.20 / 35	3.00 / 45	4.40 / 63
Distance 1D	0.10 / 0	0.31 / 0	0.40 / 4	0.46 / 11	0.65 / 21
Distance 2D	0.01 / 0	0.07 / 0	0.10 / 0	0.35 / 0	0.60 / 2

: No damage : Slight damage

: Moderate damage : Severe damage

The effects of explosive weight versus stand-off distance of the tunnel were used to plot different damage zones for two situations described in Fig. 11. Fig. 14(a) depicts the variation of damage states due to the influence of the tunnel depth, in which the stand-off distance is equal to the tunnel depth. Three critical lines are drawn using best-fitting lines to divide the boundary between different damage zones. Some intermediate coordinates were selected and relevant simulations were carried out to fine-tune the critical lines. The following equations mathematically express the relationship between the stand-off distances to the explosive weight:

$$\left.\begin{aligned} \text{Line}\,1: R &= 2.94\ln(w) - 6.78 \\ \text{Line}\,2: R &= 3.94\ln(w) - 15.02 \\ \text{Line}\,3: R &= 5.40\ln(w) - 28.42 \end{aligned}\right\} 6.35m \le R \le 12.70m \qquad \text{Eq. 3}$$

where R is the stand-off distance in m, w is the explosive weight in kg.

Line 1 illustrates the threshold border between no damage zone to slight damage zone, points on the left side of the line produces no damage in the tunnel lining. Line 2 depicts the threshold border between slight damage zone to moderate damage zone. The coordinates between Line 1 and 2 denotes that the tunnel exhibited minor cracks with few bolt failures. Under slight damage, the tunnel can return to operation after some surface repairs. The third line divides the moderate and the severe damage zones. The region between Line 2 and 3 produces moderate damage. Table 6 shows that 250kg of TNT explosive can cause moderate damage on shallow buried tunnels. In addition to deep and wider cracks, the tunnel segments suffered a large number of bolt failures causing drifting or sliding displacement between

segments. It may be considered that those affected segments are at risk of failing. Furthermore, infiltration of water and soil through the joints can alter the surrounding ground condition and speed up the damage state. This may require complete replacement of affected segments. Replacing segments are often associated with time consuming labour and in turn correspondingly cost intensive repair work.

The right side of Line 3 illustrates that the combination of explosive (w) and stand-off distance (R) resulted in very severe damage to the structural integrity of segmented lining. The most severe damage state is associated with deep and wider cracks and several bolt failures. The cracks extended from the bottom of interior surface to top of the segments due to high bending stresses developed from the explosion. Several bolt failures caused drifting between segments at the radial joints. When the drifting exceeded a certain degree, the segments lost contact hoop force transmission capacity at those radial joints. As a result, the segmented lining was subjected to progressive collapse as displayed in Fig. 12(a).

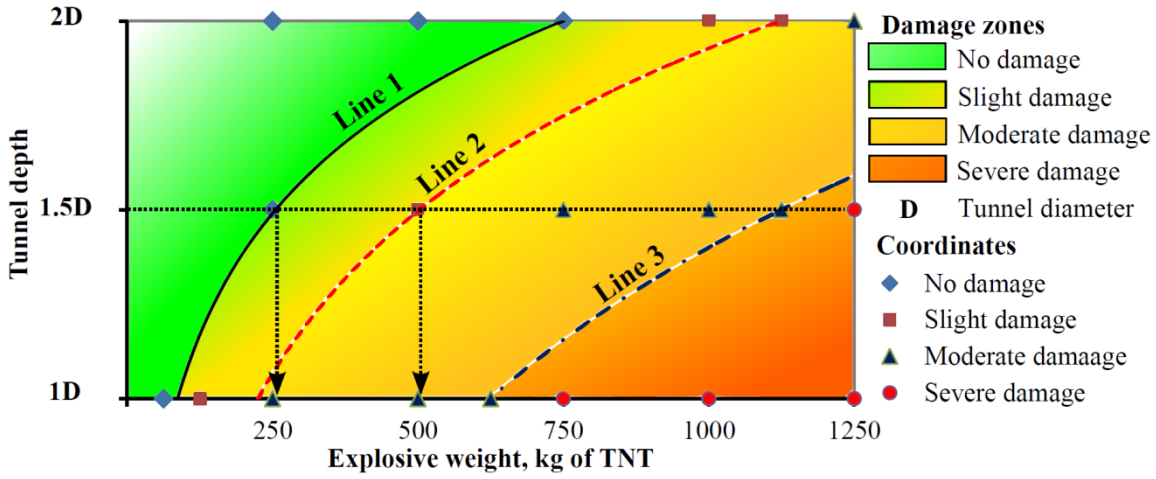

Explosive wei((a) Variation of tunnel depth

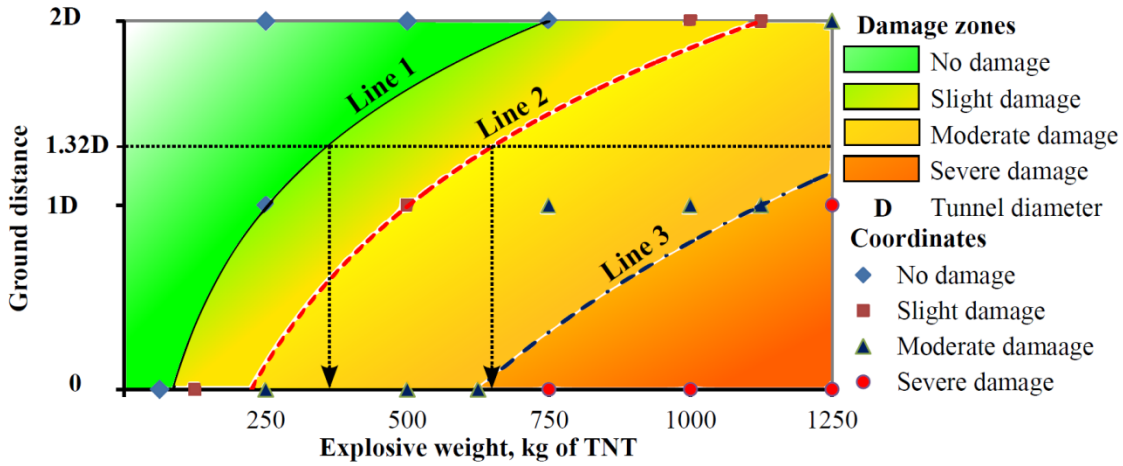

(b) Exp(b) Variation of ground distance ound distance for different

Fig. 14: Critical explosive weight vs. stand-off distance for different damage state

A ground distance of 1.32D in Fig. 14(b) is equivalent to the stand-off distance of 1.5D (tunnel depth of 1.5D in Fig. 14(a)). Two critical explosive weights for stand-off distance of 1.5D corresponding to Line 1 and Line 2 are projected as shown in Fig. 14(a). The projected values for Line 1 & 2 are 250 and 500kg of TNT respectively. Similar arrows shown in Fig. 14(b) denote that those values for Line 1 & 2 are significantly greater than 350 and 650kg of TNT respectively. For the same scaled distances, the study shows that the tunnel is more vulnerable to the surface explosion from the explosive placed on the centerline of the tunnel than any other locations on the surface. When the shockwave impacted the tunnel, the sideways component of the shockwave influenced the tunnel motion in a direction perpendicular to the ground surface. Due to shallow soil cover above the tunnel crown, the tunnel is more flexible in crown-invert direction than the lateral direction as the infinite soil medium constrains the tunnel in the lateral direction. In addition, a previous publication (16) demonstrated that shallower gauge points experienced slightly small peak pressures than the corresponding gauge points directly below the explosive.

Furthermore, Fig. 14(b) assists to develop a protection and safety zone in order to reduce detrimental effects of any possible surface explosions. Incorporation of proper and adequate precaution/protection measures by restricting any activities within the zones will protect the tunnel from credible blasts. For example, the study shows that the introduction of a safety zone 1.0D distance from the tunnel centerline completely protects the tunnel from an explosion caused by car bombs and the tunnel is even safe with slight damages if the explosion is caused by SUV/van bomb.

6. Conclusion

In this paper, a fully coupled Fluid Structure Interaction (FSI) technique incorporating the Arbitrary Lagrangian-Eulerian (ALE) method was applied to investigate the blast response of a segmented tunnel buried in different soil types using the software LS-DYNA. The modeling techniques had been validated in a previous paper (16) and are further validated in the present paper by comparing the numerical results with those from the CONWEB test (8). Three types of soils were considered first by varying the weight of explosive on the ground surface, followed by a study to predict the blast response of the segmented tunnel to different scale distances by varying the tunnel depth as well as the ground distance of explosive from the tunnel centreline. Four damage categories for the segmented tunnel lining subjected to surface blast were investigated, such as no damage, slight damage, moderate damage and severe damage. The numerical results have been mathematically transformed to develop critical lines to represent the critical explosive weight versus the stand-off distance relationships corresponding to the four damage states. The main findings of this study are as follows:

- Both soil composition and degree of water saturation have a great impact on the peak pressure response in the soil as well as the dynamic impact on the buried tunnel structure.
- The blast response of buried tunnel in saturated soil is more severe in terms of crack formation and bolt failures than that in tunnels buried in either partially saturated soil or dry soil when subjected to the same surface explosion.
- In all soil types, the diametric distortions increase with the explosive mass and the distortions are unrecoverable in all load cases (from 250 to 1250kg of TNT). As the explosive mass increased to more than 750kg of TNT, the tunnel buried in the saturated soil displayed segment-disintegration from neighbouring segments.
- The analytical curves developed in this study enable a quick and simple assessment of the vulnerability of buried tunnels subjected to surface blasts. Comparison of critical lines for identical scale distances illustrates that the tunnel lining is more vulnerable to surface explosions which occurred directly above the centre of the tunnel than those that occurred in the ground at any equivalent distances from the tunnel centre.
- For the tunnel considered in this study, the safe explosive weights for explosions that occur directly above the centre of the tunnel can be recommended: if a tunnel is buried at a depth of 6.35m, the safe explosive weight to avoid severe damage should be a

maximum of 625kg of TNT, whereas for a depth of 9.52m, the safe explosive weight is 1125kg of TNT which is almost double.

- Providing a safety zone (a distance of 6.35m on either side of the tunnel centreline) on the ground will protect the shallow buried tunnel from severe damage from up to 1125kg of TNT explosive.
- The modelling techniques used in the present research and the research findings will be useful as a benchmark for future studies in this area.

References

1. Shin JH, Moon HG, Chae SE. Effect of blast-induced vibration on existing tunnels in soft rocks. Tunnelling and Underground Space Technology. 2011;26(1):51-61.
2. De A, Morgante AN, Zimmie TF. Mitigation of Blast Effects on Underground Structure Using Compressible Porous Foam Barriers. Poromechanics V: American Society of Civil Engineers, USA; 2013. p. 971-80.
3. De A. Numerical simulation of surface explosions over dry, cohesionless soil. Computers and Geotechnics. 2012 6//;43(0):72-9.
4. Davies MCR, editor Dynamic Soil Structure Interaction Resulting from Blast Loading. Centrifuge 94 Rotterdam:Balkema; 1994.
5. Davies MCR, Williams AJ. Centrifuge Modelling the Protection of Buried Structures Subjected to Blast Loading. Structures Under Shock and Impact II. 1992:663-74.
6. Kutter BL, O'Leary LM, Thompson PY. Gravity-Scaled Tests on Blast-Induced Soil-Structure Interaction. Journal of Geotechnical Engineering,. 1988;114:431-47.
7. Whittaker JP. Centrifugal and numerical modeling of buried structures. Volume 3. A centrifuge study of the behavior of buried conduits under airblast loads. Final report. Colorado Univ., Boulder (USA). Dept. of Civil, Environmental, and Architectural Engineering, 1987.
8. Hayes PG. Backfill Effects on Response of Buried Reinforced Concrete Slabs. Vicksburg, Mississippi: Waterways Experiment Station, Corps of Engineers, 1989 SL-89-18.
9. Liu H. Soil-Structure Interaction and Failure of Cast-Iron Subway Tunnels Subjected to Medium Internal Blast Loading. Journal of Performance of Constructed Facilities. 2012;Vol. 26:691-701.
10. Yang Y, Xie X, Wang R. Numerical simulation of dynamic response of operating metro tunnel induced by ground explosion. Journal of Rock Mechanics and Geotechnical Engineering. 2010;2(4):373-84.
11. Liu H. Dynamic Analysis of Subway Structures Under Blast Loading. Geotechnical and Geological Engineering. 2009;27(6):699-711.
12. Feldgun VR, Kochetkov AV, Karinski YS, Yankelevsky DZ. Internal blast loading in a buried lined tunnel International Journal of Impact Engineering 2008;35:172 - 83.
13. Gui M, Chien M. Blast-resistant Analysis for a Tunnel Passing Beneath Taipei Shongsan Airport–a Parametric Study. Geotechnical and Geological Engineering. 2006;24(2):227-48.

14. LSTC. LS-DYNA Keyword User's Manual v971, Livermore Software Technology Corporation(LSTC). California, USA. 2007.
15. Nasri Munfah PE. Safety and Security of Tunnels and Underground Transportation Facilities. Parsons Brinckerhoff, National Tunnelling Practice Leader, New York, USA. 2009.
16. Koneshwaran S, Thambiratnam D, Gallage C. Performance of Buried Tunnels Subjected to Surface Blast Incorporating Fluid Structure Interaction. ASCE Journal of Performance of Constructed Facilities. 2014.
17. Koneshwaran S, Thambiratnam D, Gallage C, Response of segmented bored transit tunnels to surface blast, Advances in Engineering Software, ISSN 0965-9978 (in press).
18 Koneshwaran S, Thambiratnam D, Gallage C, Blast Response of Segmented Bored Tunnel using Coupled SPH–FE Method, Structures, ISSN 2352-0124(in press).
19. Lewis BA. Manual for LS-DYNA Soil Material Model 147. Federal Highway Administration, McLEAN, VA2004.
20. Saleh M, Edwards L. Application of a soil model in the numerical analysis of landmine interaction with protective structures 26th International symposium on blastics MIAMI; September 12-16: DEStech Publications, Inc., Pennsylvania, USA; 2011.
21. Jayasinghe LB, Thambiratnam DP, Perera N, Jayasooriya JHAR. Computer simulation of underground blast response of pile in saturated soil. Computers & Structures. 2013;120(0):86 - 95.
22. Lee WY. Numerical modeling of blast-induced liquefaction: Department of Civil and Environmental Engineering, Brigham Young University, USA; 2006.
23. Ortman, Catherine M. The Effect of Diameter on Dynamic Seabed Penetration. NAVAL ACADEMY ANNAPOLIS MD, 2008 Contract No.: Trident Scholar Project rept. no. 373.
24. Bessette GC. Modeling Coupled Blast/Structure Interaction with Zapotec, Benchmark Calculations for the Conventional Weapon Effects Backfill (CONWEB) Tests. Sandia National Laboratories Report SAND20044096, 2004.
25. Baylor JT. Parameters Affecting Loads on Buried Structures Subjected to Localized Blast Effects. Army Engineer Waterways Experiment Station Vicksburg Ms Structures Lab, 1992 Contract No.: ADA261365.
26. Ottosen NS. A Failure Criterion for Concrete. Journal of Engineering Mechanics Division. 1977;103(4):527-35.
27. Darwin D, Barham S, Kozul R, Luan S. Fracture energy of high-strength concrete. ACI Materials Journal. 2001;98(5).
28. Oluokun, Francis A, Edwin G. Burdette, Deatherage JH. Young's modulus, Poisson's ratio and compressive strength relationships at early ages. ACI Materials Journal. 1991;88:3-9.
29. Jayasinghe LB, Thambiratnam D, Perera NJ, Jayasooriya R. Effect of Soil Properties on the Response of Pile to Underground Explosion. Structural Engineering International. 2014 //;24(3):361-70.
30. Dazhi Wen, John Poh, Ng YW. Design considerations for bored tunnels at close proximity. Tunnelling and Underground Space Technology. 2004 7//;19(4–5):468-9.
31. Civil Design Criteria for Road and Rail Transit Systems. Engineering Group, Land Transport Authority, Singapore, 2010 Contract No.: E/GD/09/106/A1